Available online at www.sciencedirect.com
ScienceDirect
International Journal of Thermal Sciences 47 (2008) 1347–1358
International Journal of Thermal Sciences
www.elsevier.com/locate/ijts

Artificial neural network models for predicting soil thermal resistivity

Yusuf Erzin [a], B. Hanumantha Rao [b], D.N. Singh [b,*]

[a] *Department of Civil Engineering, Celal Bayar University, 45140 Manisa, Turkey*
[b] *Department of Civil Engineering, Indian Institute of Technology Bombay, Mumbai-400076, India*

Received 22 June 2007; received in revised form 1 November 2007; accepted 2 November 2007

Available online 20 February 2008

Abstract

Thermal properties of soils are of great importance in view of the modern trends of utilizing the subsurface for transmission of either heated fluids or high power currents. For these situations, it is essential to estimate the resistance offered by the soil mass in dissipating the heat generated through it. Several investigators have tried to develop mathematical and theoretical models to estimate soil thermal resistivity. However, it is evident that these models are not efficient enough to predict accurate thermal resistivity of soils. This is mainly due to the fact that thermal resistivity of soils is a complex phenomenon that depends upon various parameters viz., type of the soil, particle size distribution and its compaction characteristics (i.e., dry density and moisture content). To overcome this, Artificial Neural Network (ANN) models, which are based on experimentally obtained thermal resistivity values for clay, silt, silty-sand, fine- and coarse-sands, have been developed. Incidentally, these soils are the most commonly encountered soils in nature and exhibit entirely different characteristics. The thermal resistivity of these soils, corresponding to their different compaction states, was obtained with the help of a laboratory thermal probe and compared vis-à-vis those obtained from the ANN model. The thermal resistivity of these soils obtained from ANN models and experimental investigations are found to match extremely well. The performance indices such as coefficient of determination, root mean square error, mean absolute error, and variance account for were used to control the performance of the prediction capacity of the models developed in this study. In addition to this, thermal resistivity of these soils obtained from ANN models were compared with those computed from the empirical relationships reported in the literature and were found to be superior. The study demonstrates the utility and efficiency of the ANN model for estimating thermal resistivity of soils.

Keywords: Soils; Thermal resistivity; Empirical relationships; Laboratory investigations; Artificial neural network

1. Introduction

Soil resistivity is a complex property that depends mainly on the type of the soil, moisture content, particle size distribution, and closeness of packing of the grains. The type of soil is considered to be an important factor for determining its thermal resistivity [1,2]. It has also been demonstrated that soil resistivity is affected easily by the conditions in which it is formed [3].

Since the conduction through soil is largely electrolytic, the amount of water present in soil plays an important role in determining its resistivity [2]. Normally, dry soils depict low conductivity [2], mainly due to the presence of air (a poor conductor and its resistivity value being 4000 °C cm/Watt), which separates the solid grains (resistivity equal to 4 °C cm/Watt) of the soil. If the moisture content (for water, the resistivity value is 165 °C cm/Watt) of the soil increases, its conductivity increases [1]. As such, a saturated soil has high conductivity as compared to the water [4].

It has been demonstrated by earlier researchers that the soil thermal resistivity at first falls rapidly as moisture content increases, however, after achieving the critical moisture content, it attains almost a constant value [5,6]. This is best accomplished with well-graded sand to fine gravel (sound mineral rock), with a small percentage of fines (silt and clay), that can be easily compacted to a high density [7]. For maximum density the smaller grains efficiently fill the spaces between the larger particles, and the fines enhance the moisture retention [1]. A sound mineral aggregate, without organics, and without porous particles, ensures effective thermal conduction. The particle size and its distribution also have an effect on the manner in which

* Corresponding author.
E-mail addresses: yusuf.erzin@bayar.edu.tr (Y. Erzin), hanuma_bendadi@iitb.ac.in (B.H. Rao), dns@civil.iitb.ac.in (D.N. Singh).

1290-0729/$ – see front matter
doi:10.1016/j.ijthermalsci.2007.11.001

Nomenclature

γ_d	dry unit weight of the soil
μ	momentum factor
ρ	resistance per unit length
b	parameter
D	particle diameter ..... mm
D_{10}	particle diameter finer than 10%
D_{30}	particle diameter finer than 30%
D_{50}	particle diameter finer than 50%
D_{70}	particle diameter finer than 70%
e_{max}, e_{min}	maximum and minimum void ratio, respectively
G	specific gravity
H_1, H_2, H_3	input elements
i	current
MAE	mean absolute error
N	number of the samples
N_{hl}	number of neurons in the hidden layer
Q	heat input
R_1	output element
$RMSE$	root mean square error
R_T	thermal resistivity ..... °C cm/Watt
$R_{T(ANN)}$	thermal resistivity estimated from ANN model ..... °C cm/Watt
$R_{T(Expt.)}$	experimentally obtained thermal resistivity ..... °C cm/Watt
VAF	variance account for
var	variance
w	water content ..... %
x	actual value
x_{max}	maximum value
x_{min}	minimum value
x_{norm}	normalized value
y	measured value
$\hat{y}$	predicted value
Y_i, Y_j	hidden neurons

the moisture is held. With large sized grains, the pore space available will be higher (due to the presence of air) resulting in higher resistivity or lower conductance [4]. However, for well-graded soil, higher soil density can be achieved by compaction (the space between the large grains becomes occupied by the smaller ones) and hence they exhibit less resistivity. Also, if the size and shape of the grains are in such a way that they form a compact dense structure then the resistivity of the soil decreases [1].

Various investigators have made attempts to develop relationships to estimate thermal resistivity of soils by taking into account its different physico-chemical properties. In general, these relationships can broadly be categorized under two groups: (1) empirical relationships that are based on data obtained by measurements; and (2) theoretical equations, which are based on idealized models wherein the actual soil structure is simplified. However, these relationships suffer from limitations in terms of proper incorporation of various factors affecting a complex mechanism like soil thermal resistivity [4,6,7].

In recent years, Artificial Neural Networks (ANNs) has been employed, quite frequently, as a promising tool for supporting the modeling of complicated systems, which incorporate multiple parameters or variables [8,9]. An ANN presents a computational mechanism that is able to acquire, represent and compute a mapping from one multivariate space of information to another, given a set of data representing that mapping.

With this in mind, an attempt was made to develop ANN models for predicting thermal resistivity of soils and these details are presented in this paper. To achieve this, the thermal resistivity of clay, silt, silty-sand, fine- and coarse-sands, compacted to various dry densities and moisture contents, were measured using a laboratory thermal probe. To demonstrate the efficiency of the ANN models, the results obtained were compared with those obtained from experimental investigations and empirical relationships, which are reported in the literature.

2. Details of the neural network

An Artificial Neural Network (ANN), by means of its architecture, attempts to simulate the biological structure of the human brain and nervous system [10–12]. This network consists of three or more layers; an input layer, one or more hidden layers, and an output layer. Each layer consists of a number of interconnected processing elements, commonly referred to as neurons. These neurons interact with each other via weighted connections. Each neuron is connected to all the neurons in the next layer. In the input layer, data are presented to the neural network, while the output layer holds the response of the network to the input. The hidden layers enable these networks to represent and compute complicated associations between inputs and outputs. This ANN architecture is commonly referred to as a fully interconnected feed-forward multi-layer perceptron (MLP). A typical ANN architecture consisting of H_1, H_2 and H_3 as the input elements, Y_i and Y_j as the hidden neurons and R_1 as the output, is depicted in Fig. 1.

The usage of a number of hidden layers in the ANN depends on the degree of complexity in the pattern recognition problem, and one or two hidden layers are found to be quite useful for most problems [13–15]. Also, the number of neurons in the

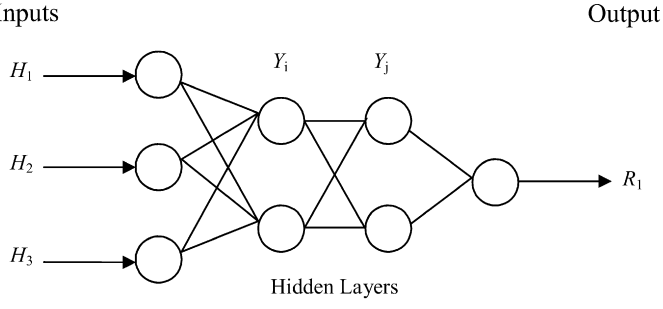

Fig. 1. The ANN architecture.

hidden layers depends on the nature of the problem, and various methods have been employed by several researchers to determine them [16–21]. However, these methods present general guidelines only for selection of an adequate number of neurons.

The most popular neural-network paradigm is the back-propagation learning algorithm [14,21–26]. The back-propagation neural network has been applied with great success to model many phenomena in the field of geotechnical and geoenvironmental engineering [27–31]. Each hidden and output neuron processes its input(s) by multiplying each by its weight, summing the product, and then processing the sum using a nonlinear transfer function, (also called an 'activation function'), to obtain the desired result. The most common transfer function implemented in the literature is the sigmoid function. The neural network "learns" by modifying the weights of the neurons in response to the errors between the actual output values and the target output values. This is carried out through gradient descent on the sum of the squares of the errors for all the training patterns [22,27]. The changes in the weights are proportional to the negative of the derivative of the error term. One pass through the set of training patterns, together with the associated updating of the weights, is called a cycle or an epoch. Training is carried out by repeatedly presenting the entire set of training patterns (updating the weights at the end of the each epoch) until the average sum squared error over all the training patterns is minimal and within the tolerance specified for the problem.

At the end of the training phase, the neural network should correctly reproduce the target output values for the training data; provided errors are minimal (i.e. convergence occurs). The associated trained weights of the neurons are then stored in the neural network memory. In the next phase, the trained neural network is fed a separate set of data. In this testing phase, the neural network predictions using the trained weights are compared to the target output values. The performance of the overall ANN model can be assessed by several criteria [32–35]. These criteria include coefficient of determination R^2, root mean squared error, mean absolute error, minimal absolute error, maximum absolute error and variance account for. A well-trained model should result in an R^2 value close to 1 and small values of error terms.

In this study, the prediction of thermal resistivity of soils has been modeled using the ANN in which network training was accomplished with the neural network toolbox written in Matlab environment [36]. The Levenberg–Marquardt back-propagation learning algorithm [36] was used in the training stage. Details of the experimental investigations, which have yielded the data used in ANN models, are presented in the following section.

3. Experimental investigations

Soils such as clay (black cotton soil), silt (fly ash), silty-sand, fine-sand and coarse-sand were selected for the present study for their thermal resistivity measurements at different densities and moisture contents [37]. These soils were characterized for their physical and index properties, as depicted in Table 1, and their gradational characteristics are presented in Fig. 2.

A thermal probe, which operates on the "Transient method" [38,39], was fabricated and used in this study. As depicted in Fig. 3, the probe consists of an insulated Nichrome heater wire of resistance, ρ (= 0.19 Ω/cm), inserted in a copper tube of 140 mm length and external diameter equal to 2.5 mm. A thermocouple is attached on the surface of the tube as shown in

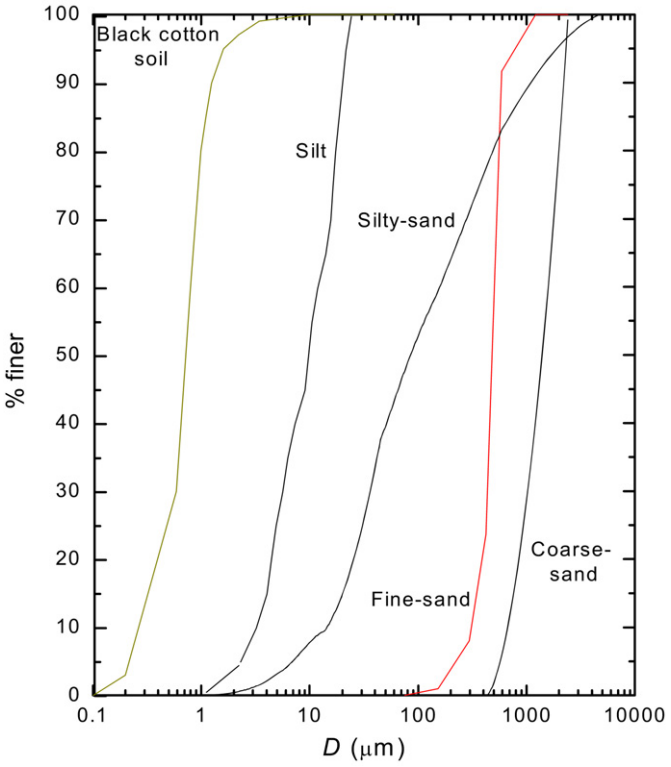

Fig. 2. Gradational characteristics of the soils used in the study.

Table 1
Properties of the soils used in the present study

Soil property	Block cotton	Silt (fly ash)	Silty-sand	Fine-sand	Coarse-sand
G	2.72	2.14	2.78	2.63	2.65
Clay fraction (%)	96	10	1	0	0
Silt fraction (%)	4	90	47	0	0
Sand fraction (%)	0	0	52	100	100
Liquid limit (%)	67	–	41	–	–
Plastic limit (%)	34	–	28	–	–
USCS	CL	CL	SC	–	–
e_{max}	–	–	–	0.781	0.765
e_{min}	–	–	–	0.540	0.623

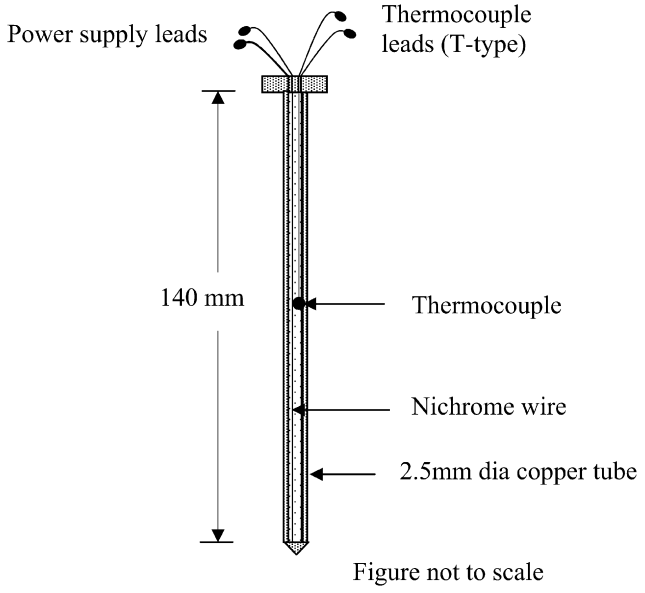

Fig. 3. The thermal probe.

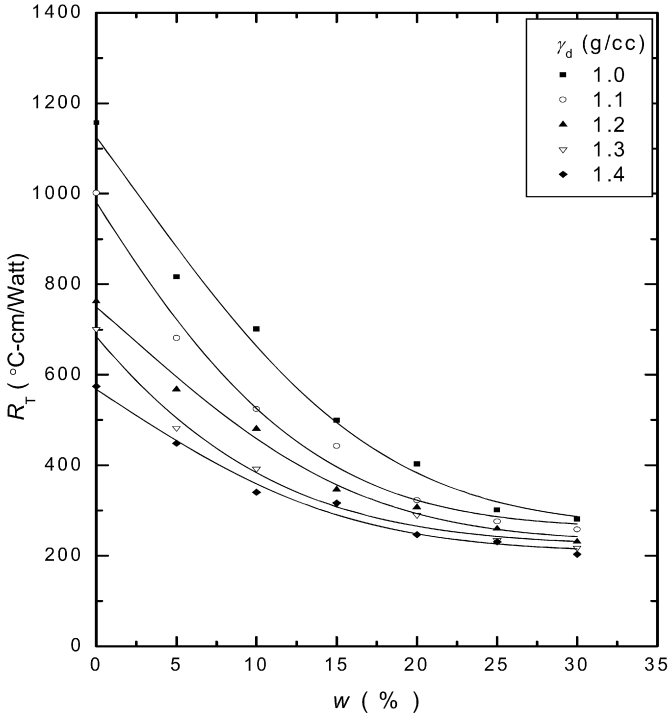

Fig. 4. Variation of thermal resistivity with moisture content for the black cotton soil.

the figure. The heat input per unit length, Q, is equal to i^2. ρ (in Watt/cm), where, i is the current passing in the heater wire. The calibration of this probe was achieved by using a standard liquid glycerol with thermal resistivity, R_T, equal to 349 °C cm/Watt [37,40]. The R_T of the glycerol is found to be equal to 357 °C cm/Watt (for $i = 0.5$ Amp), which is only 2.4% higher than its standard value. A metal container (150 mm long and 100 mm diameter) was used to prepare the soil samples corresponding to a particular density and moisture content. A 2 mm-diameter hole was drilled in the soil sample and the

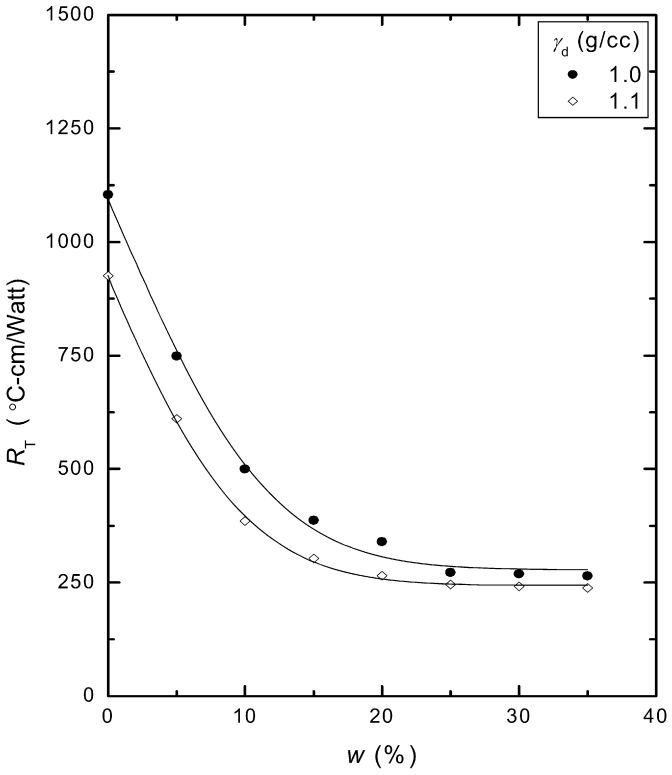

Fig. 5. Variation of thermal resistivity with moisture content for the silt.

thermal probe was fitted tightly into it. The probe was allowed to achieve thermal equilibrium in the soil mass for some time (5 min approx.) and then the power supply to the probe was switched on. The temperature of the probe was recorded as a function of time and was used to compute the thermal resistivity of the soil.

The variation of R_T with water content, w, for the clay, silt, silty-sand, fine- and coarse-sands is presented in Figs. 4 to 8, respectively, for the achieved dry density, γ_d, values. It can be observed from these figures that, in general, the resistivity decreases as the moisture content of the soil increases, for a given compaction state of the soil. As water is added to the soil, it forms a thin film on the soil particles which eases the flow of heat. This may be attributed to the fact that the thermal resistivity of air (= 4000 °C cm/Watt) is higher than that of water (= 165 °C cm/Watt). Further, addition of moisture to the soils results in replacement of air in the voids (and hence the density increases) by the pore water thus reducing the thermal resistivity of the soil in the near vicinity of its optimum moisture content (OMC). As such, the soil attains almost a constant resistivity value that is the minimum resistivity it can exhibit. A reduction in the thermal resistivity of the soil has been observed with increasing density, from the resistivity curves. This is due to the improvement in contact between soil particles, which leads to better conduction of heat.

4. Development of ANN models

As discussed earlier, soil parameters viz., type, gradational characteristics, moisture content and dry density, greatly affect

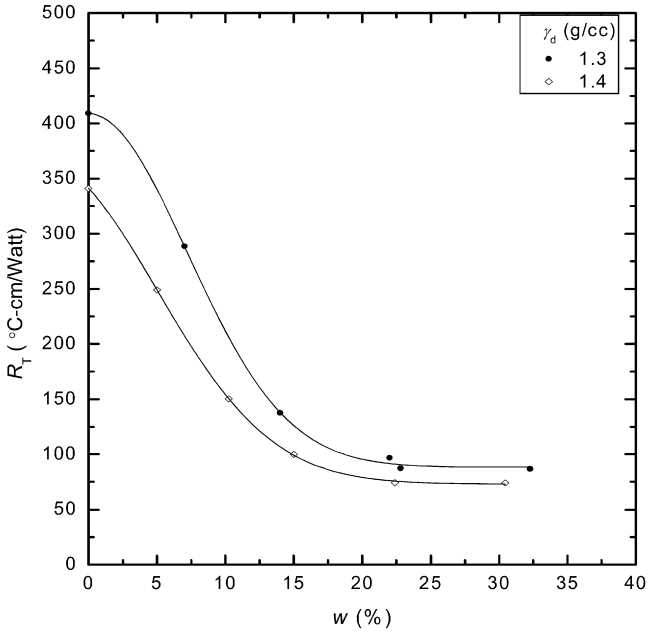

Fig. 6. Variation of thermal resistivity with moisture content for the silty-sand.

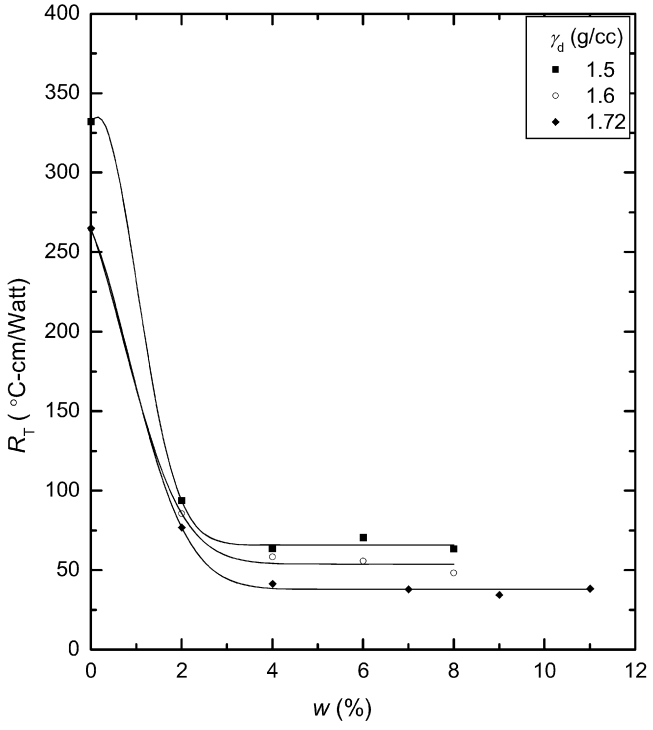

Fig. 7. Variation of thermal resistivity with moisture content for the fine-sand.

its thermal resistivity. Therefore, ANN models were developed independently for clay (designated as ANN-C), silt (ANN-S), silty-sand (ANN-SS), fine- and coarse-sands (ANN-FS and ANN-CS), respectively. In addition, a generalized ANN model (ANN-G), which accounts for different soils compacted to different states was developed by using the experimental data. Individual ANN models have two input parameters (w and γ_d), while, the ANN-G model has six input parameters (D_{10}, D_{30}, D_{50}, D_{70}, w and γ_d). All these models have one output parameter R_T. The boundaries for input and output parameters of the models are listed in Tables 2 and 3. The input–output data of each ANN model were scaled to lie between 0 and 1 by using Eq. (1).

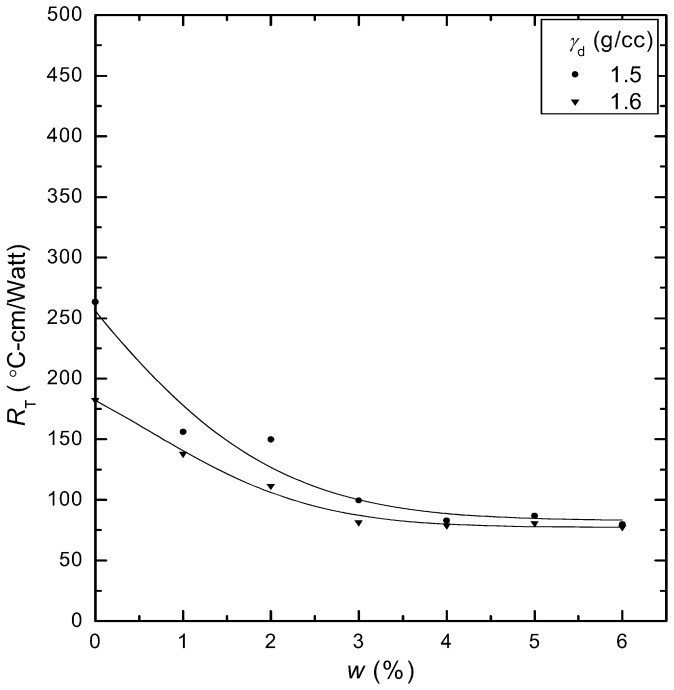

Fig. 8. Variation of thermal resistivity with moisture content for the coarse-sand.

Table 2
Boundaries of the input and output parameters used for developing ANN models for individual soils

Model	Input parameter				Output parameter	
	w (%)		γ_d (g/cc)		R_T (°C cm/Watt)	
	Min.	Max.	Min.	Max.	Min.	Max.
ANN-C	0	30	1.0	1.4	203	1157
ANN-S	0	35	1.0	1.1	238	1104
ANN-SS	0	32	1.3	1.4	73	409
ANN-FS	0	11	1.5	1.72	34	332
ANN-CS	0	6	1.5	1.6	77	276

Table 3
Boundaries of the input and output parameters for the model ANN-G

Parameter	Symbol	Min.	Max.
Input	D_{10} (mm)	0.2	670
	D_{30} (mm)	0.6	1000
	D_{50} (mm)	0.7	1425
	D_{70} (mm)	0.8	1775
	w (%)	0	35
	γ_d (g/cc)	1	1.7
Output	R_T (°C cm/Watt)	34	1157

$$x_{norm} = \frac{(x - x_{min})}{(x_{max} - x_{min})} \tag{1}$$

where x_{norm} is the normalized value, x is the actual value, x_{max} is the maximum value and x_{min} is the minimum value.

It is a common practice to divide the available data into two subsets; a training set, to construct the neural network model, and an independent validation set to estimate model performance in the deployed environment [41]. However, dividing the data into only two subsets may lead to model over fitting. Over fitting makes multi-layer perceptrons (MLPs) memorize training patterns in such a way that they cannot generalize well to new data [34]. As a result, the cross validation technique [42] was used as the stopping criterion in this study. In this technique, the database is divided into three subsets: training, validation and testing. The training set is used to update the networks' weights. During this process the error with the validation set is monitored. When the validation set error begins to increase, training is stopped because it is considered to be the best point of generalization. Finally, the testing data are fed into the networks to evaluate their performance. Therefore, in total, 56% of the data were used for training, 24% for testing, and 20% for validation for each model developed in this study.

It has been shown that a network with one hidden layer can approximate any continuous function, provided that sufficient connection weights are used [43]. Consequently, one hidden layer was used in all the models. The neural network toolbox of MATLAB7.0, a popular numerical computation and visualization software [34], was used for training and testing of MLPs. The optimum number of neurons in the hidden layer of each model was determined by varying their number by starting with a minimum of 1 and then increasing the network size in steps by adding 1 neuron each time. Different transfer functions (such as log-sigmoid [44] and tan-sigmoid [13]) were investigated to achieve the best performance in training as well as in testing. Two momentum factors, μ (= 0.01 and 0.001), were selected for the training process to search for the most efficient ANN architecture; the maximum number of training epochs to train was chosen as 1000. The coefficient of determination R^2 and the mean absolute error *MAE* were used to evaluate the performance of the developed ANN models. The performance of the network during the training and testing processes was examined for each network size until no significant improvement occurred.

The detailed information about the optimal performance of different ANN models is presented in Table 4. Connection weights and biases for different ANN models are presented in Tables 5 and 6. A comparison of experimental results with the results obtained from different ANN models, for training, validation, and testing samples, is depicted in Figs. 9 to 14. It can be noted from these figures that, in general, R_T values obtained from ANN models are quite close to the experimentally obtained R_T values. This shows that the ANN models are able to predict thermal resistivity of different types of soils quite efficiently.

5. Performance assessment of ANN models

The data measured and predicted from ANN models are depicted in Figs. 9 to 14. In fact, the coefficient of correlation between the measured and predicted values is a good indicator to check the prediction performance of the model [45]. In this study, variance account for (*VAF*), represented by Eq. (2), and the root mean square error (*RMSE*), represented by Eq. (3), were also computed to check the performance of the developed models [46–50].

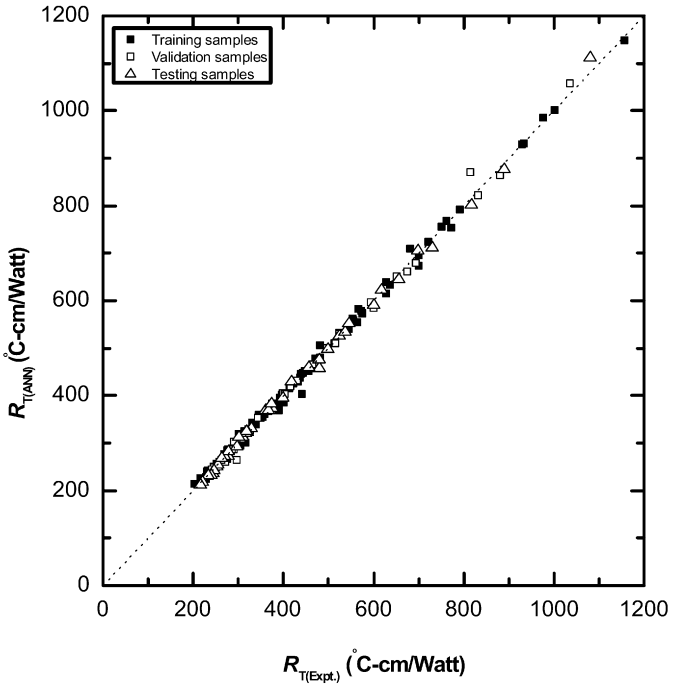

Fig. 9. Comparison of experimental results with the results obtained from the model ANN-C.

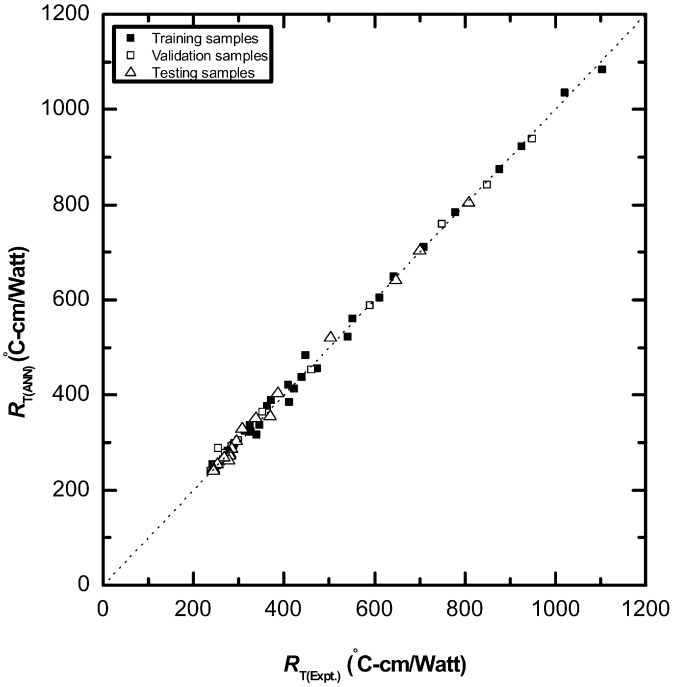

Fig. 10. Comparison of experimental results with the results obtained from the model ANN-S.

$$VAF = \left[1 - \frac{\mathrm{var}(y - \hat{y})}{\mathrm{var}(y)}\right] \times 100 \quad (2)$$

Table 4
Details of the optimal ANN performance for different ANN models

Model	Number of dataset used for			N_{hl}	Transfer function in		μ
	Training	Testing	Validation		neurons of the hidden layer	neuron of the output layer	
ANN-C	97	40	34	7	Tan-sigmoid	Log-sigmoid	0.01
ANN-S	42	18	15	9	Log-sigmoid	Log-sigmoid	0.01
ANN-SS	42	18	15	8	Log-sigmoid	Log-sigmoid	0.001
ANN-FS	56	24	20	6	Log-sigmoid	Log-sigmoid	0.001
ANN-CS	32	12	12	5	Log-sigmoid	Log-sigmoid	0.001
ANN-G	269	112	96	8	Log-sigmoid	Log-sigmoid	0.001

Table 5
Connection weights and biases of different ANN models for individual soils

Model	Hidden neuron	Weight			Bias	
		Input neuron		Output neuron	Hidden layer	Output layer
		w	γ_d	R_T		
ANN-C	1	−2.172	5.140	0.776	1.309	3.379
	2	3.535	4.567	−1.768	−7.991	
	3	2.369	−0.660	−1.277	−0.625	
	4	1.409	7.622	−0.830	−1.891	
	5	2.380	5.461	−0.566	−4.477	
	6	−7.802	−2.255	6.407	−0.684	
	7	−5.639	2.101	0.339	−1.563	
ANN-S	1	4.217	16.104	−1.357	−3.758	−14.192
	2	14.851	−8.853	4.534	−12.906	
	3	−17.493	5.725	0.332	7.990	
	4	−17.616	18.521	9.298	−0.872	
	5	−11.082	−12.893	8.519	11.679	
	6	−19.438	11.021	2.465	−0.821	
	7	−21.358	0.326	1.495	4.720	
	8	−4.772	−16.248	4.588	3.975	
	9	−11.427	−12.245	−0.850	0.726	
ANN-SS	1	−5.175	−5.745	−0.004	9.692	2.714
	2	6.085	5.660	−0.116	−7.952	
	3	8.052	−0.238	−0.008	−5.285	
	4	3.903	6.770	0.090	−6.155	
	5	−8.090	−1.511	0.080	3.678	
	6	−7.843	−1.124	0.342	1.953	
	7	−7.873	−0.859	0.540	−0.240	
	8	−8.274	−1.983	1.720	−0.246	
ANN-FS	1	−0.834	−9.103	−1.700	19.376	0.787
	2	12.045	−7.015	0.481	−3.095	
	3	−8.675	−9.578	2.334	11.652	
	4	−12.407	5.648	1.052	−0.853	
	5	10.306	−4.657	−4.023	4.925	
	6	−11.746	−1.933	12.314	−0.380	
ANN-CS	1	−10.875	−6.225	1.883	15.476	10.172
	2	0.023	12.439	−12.128	−5.687	
	3	25.371	−18.358	−12.159	1.587	
	4	6.769	5.3656	−3.711	−3.257	
	5	−6.161	10.836	3.948	−8.749	

$$RMSE = \sqrt{\frac{1}{N}\sum_{i=1}^{N}(y_i - \hat{y}_i)^2} \tag{3}$$

where var denotes the variance, y is the measured value, $\hat{y}$ is the predicted value, and N is the number of the sample. If *VAF* is 100% and *RMSE* is 0, the model is treated as excellent.

Values of *VAF* and *RMSE* for different ANN models are listed in Table 7, and it can be observed that the individual models and the generalized model are quite efficient in predicting soil thermal resistivity, as their R^2 are very close to unity. In addition, experimental results were compared with the results of the individual ANN models (Figs. 15 and 16), and with the results of the generalized model ANN-G (Figs. 17 and 18) for samples used for testing. From Figs. 15 to 18, it can be noted that the individual models as well as the generalized model predict thermal resistivity of the soil quite accurately.

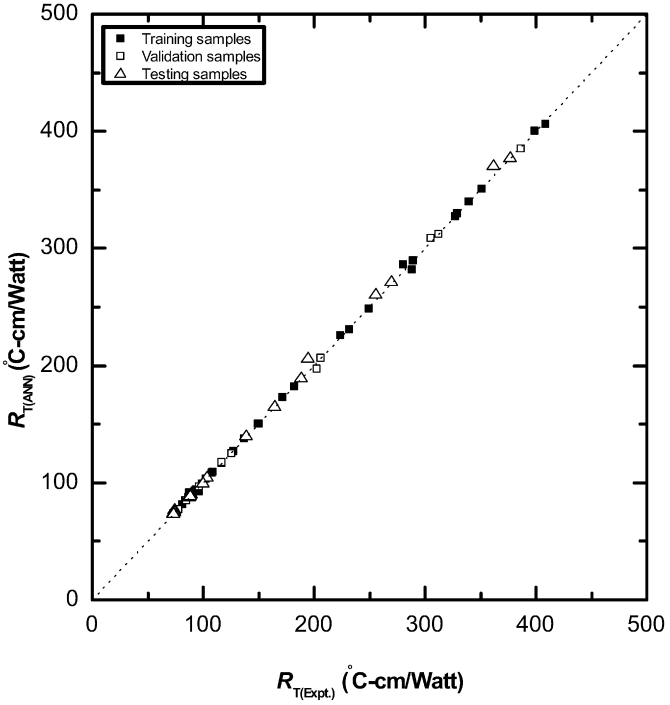

Fig. 11. Comparison of experimental results with the results obtained from the model ANN-SS.

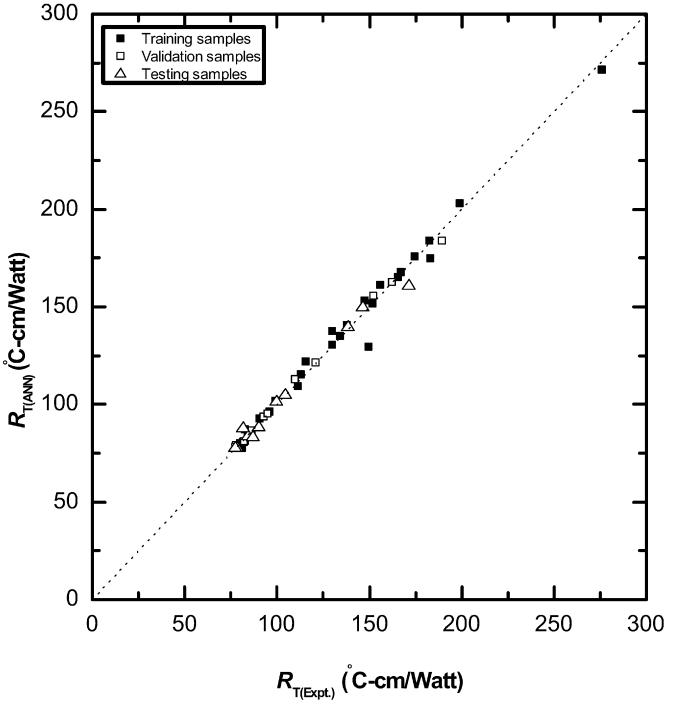

Fig. 13. Comparison of experimental results with the results obtained from the model ANN-CS.

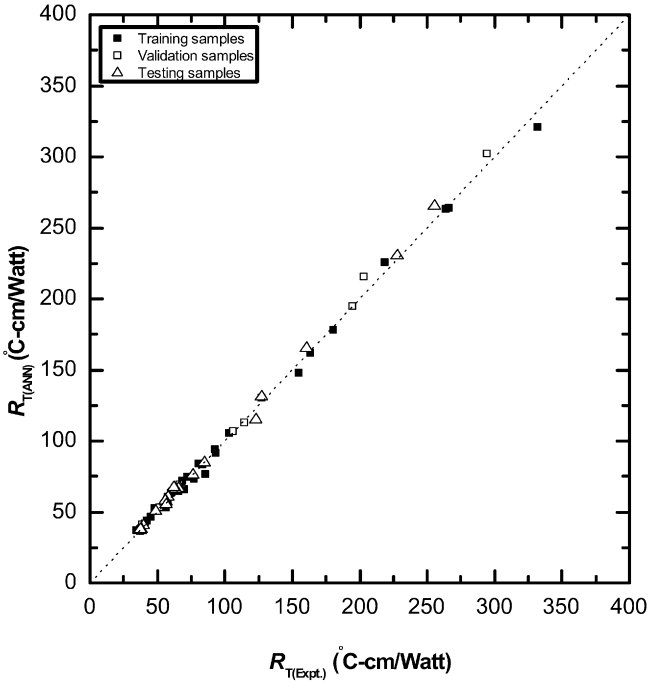

Fig. 12. Comparison of experimental results with the results obtained from the model ANN-FS.

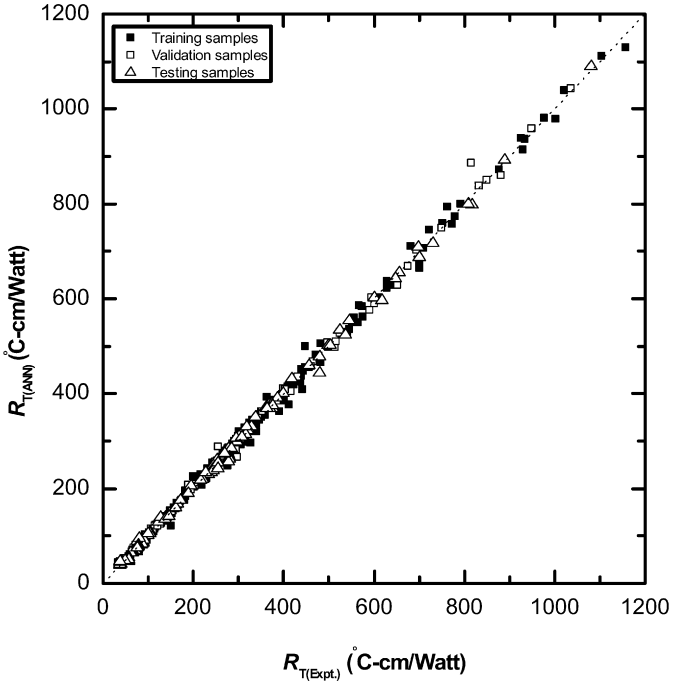

Fig. 14. Comparison of experimental results with the results obtained from the model ANN-G.

6. Comparison of ANN results with empirical relationships

Eqs. (4) and (5) are traditional methods used for predicting the soil thermal resistivity [1]. In these equations, the thermal resistivity, R_T, is in °C cm/Watt; water content, w, is in percent of dry soil weight and γ_d is the dry unit weight of the soil (in lb/ft^3).

For silt and clay soils ($w \geqslant 7\%$):

$$R_T = [1.3 \times \log w + 0.29]^{-1} \times 10^{(3-0.01\cdot\gamma_d)} \quad (4)$$

For sandy soils ($w \geqslant 1\%$):

$$R_T = [1.01 \times \log w + 0.58]^{-1} \times 10^{(3-0.01\cdot\gamma_d)} \quad (5)$$

Table 6
Connection weights and biases of the model ANN-G

Hidden neuron	Weight							Bias	
	Input neuron						Output neuron	Hidden layer	Output layer
	D_{10}	D_{30}	D_{50}	D_{70}	w	γ_d	R_T		
1	2.856	3.309	3.568	1.897	12.367	−0.675	13.391	0.296	0.296
2	−6.525	−14.043	−17.558	−17.360	−6.658	3.416	3.502	1.916	
3	8.172	4.840	3.975	5.698	−17.997	3.892	−6.765	−8.792	
4	9.326	5.798	2.153	−12.117	−22.938	−8.809	13.805	−2.086	
5	9.321	8.677	6.162	14.907	−6.388	4.229	−3.012	1.565	
6	−9.646	−14.947	−12.187	−19.368	−2.201	−4.250	13.537	−2.197	
7	0.570	−9.533	3.192	8.239	11.585	−0.555	−15.342	0.346	
8	−9.548	−2.444	0.395	18.549	−2.479	−1.953	8.300	−1.826	

Table 7
Performance indices for different ANN models

Model	Data	R^2	*RMSE* (°C cm/Watt)	*MAE* (°C cm/Watt)	*VAF* (%)
ANN-C	Training set	0.9979	9.27	6.22	99.79
	Testing set	0.9982	9.02	5.88	99.81
	Validation set	0.9959	13.53	8.02	99.58
ANN-S	Training set	0.9973	11.83	7.88	99.73
	Testing set	0.9961	10.51	8.10	99.73
	Validation set	0.9978	12.60	9.18	99.76
ANN-SS	Training set	0.9997	1.77	0.91	99.97
	Testing set	0.9993	3.19	1.57	99.91
	Validation set	0.9999	0.87	0.56	99.99
ANN-FS	Training set	0.9979	2.92	1.84	99.78
	Testing set	0.9977	3.19	2.06	99.71
	Validation set	0.9985	2.69	1.78	99.84
ANN-CS	Training set	0.9889	4.88	3.09	98.89
	Testing set	0.9824	3.99	2.55	98.31
	Validation set	0.9964	2.32	1.92	99.63
ANN-G	Training set	0.9979	10.24	6.82	99.79
	Testing set	0.9986	7.99	5.59	99.86
	Validation set	0.9979	10.90	6.36	99.78

Table 8
Value of the parameter b

Soil type	b
Clay	−0.73
Silt	−0.54
Silty-sand	0.12
Fine-sand	0.70
Coarse-sand	0.73

Eq. (6) has been developed by researchers [37] based on the experimental results of different soils, which were tested for their thermal resistivity by using a laboratory thermal probe. In this equation, parameter b is noticed to be dependent on the type of the soil, as listed in Table 8. The proposed expression is valid for, $w \geqslant 10\%$ for clays and silts, and $w \geqslant 1\%$ for sands.

$$R_T = [1.07 \times \log w + b]^{-1} \times 10^{(3-0.01\cdot\gamma_d)} \quad (6)$$

ANN results $R_{T(ANN)}$ for clay and silt samples with $w \geqslant 10\%$ used for testing the individual models ANN-C, ANN-S and generalized model ANN-G were compared with the R_T values obtained by using Eqs. (4) and (6), as depicted in Figs. 19 and 20. It can be observed from these figures that the ANN models yield better matching with the experimentally obtained thermal resistivity values $R_{T(Expt.)}$, as compared to those obtained by using these equations. Similarly, ANN results of the silty-sand, fine- and coarse-sand samples with $w \geqslant 1\%$ used for testing in individual models ANN-SS, ANN-FS and ANN-CS and generalized model ANN-G were compared with the values obtained by using Eqs. (5) and (6), as depicted in Figs. 21 and 22. It can be observed from these figures that ANN models yield better matching with the experimentally obtained R_T values, as compared to those obtained by using Eqs. (5) and (6). It can also be noted from Figs. 19 to 22 that R_T values obtained by using Eq. (6), developed for individual soils, are closer to the measured values than those obtained by using Eqs. (4) and (5). This indicates the importance of parameter b (listed in Table 8) in Eq. (6), which is dependent on the soil type [6]. This further demonstrates that the two input parameters (w and γ_d) appearing in Eqs. (4) and (5) are not sufficient enough to predict the R_T values for a given soil.

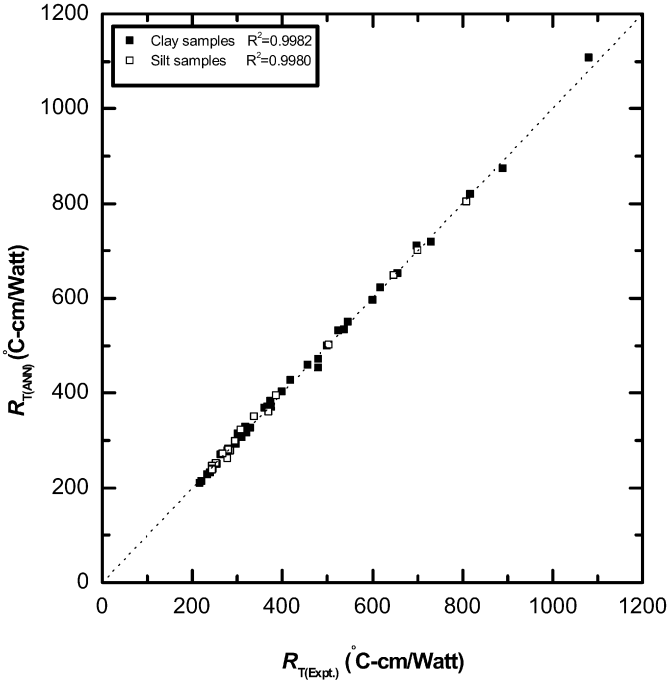

Fig. 15. Comparison of experimental results with the results obtained from models ANN-C and ANN-S.

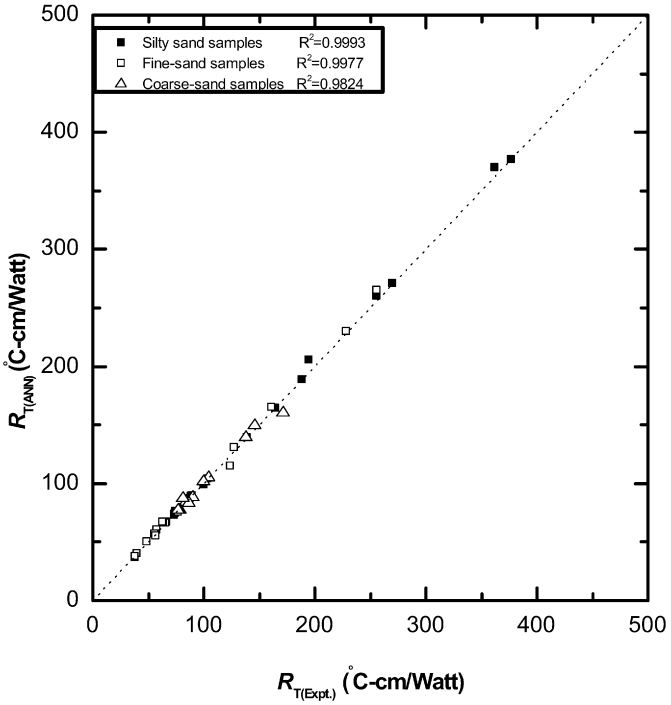

Fig. 16. Comparison of experimental results with the results obtained from models ANN-SS, ANN-FS and ANN-CS.

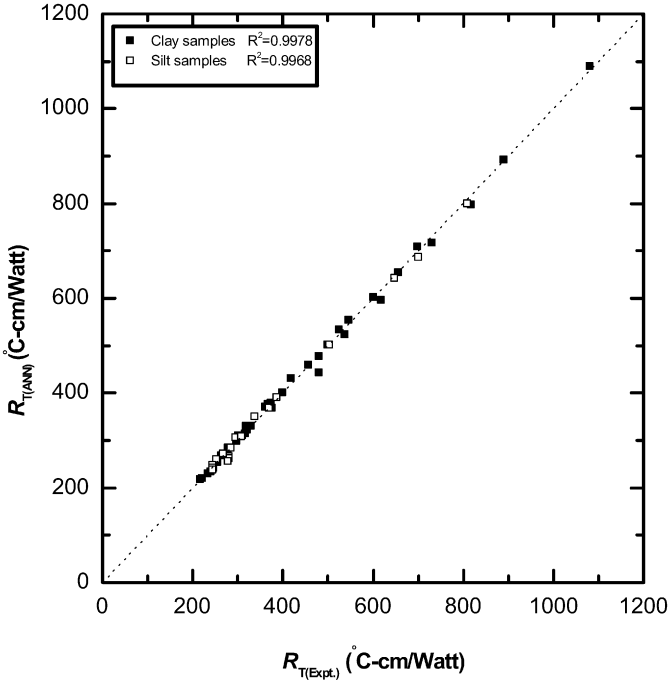

Fig. 17. Comparison of experimental results with the results obtained from the model ANN-G for clay and silt samples.

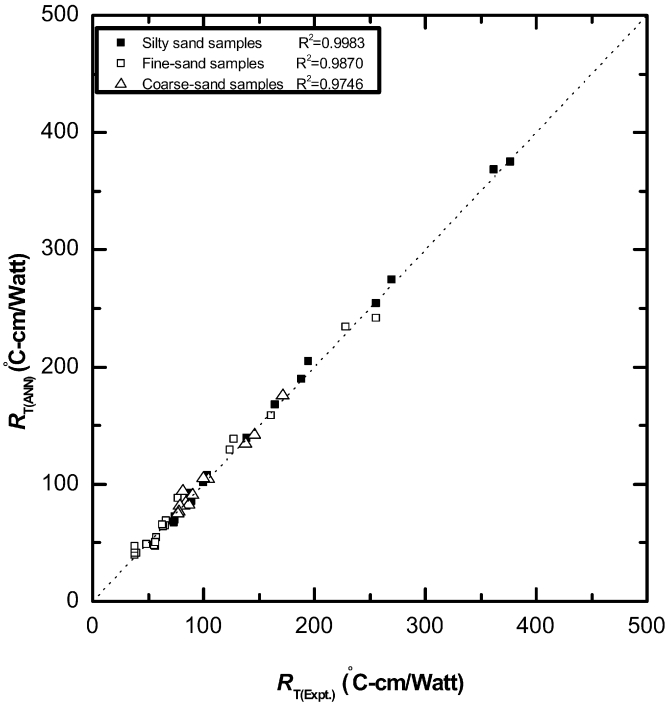

Fig. 18. Comparison of experimental results with the results obtained from the model ANN-G for silty-sand, fine-, and coarse-sand samples.

7. Conclusions

In this study, ANN models that can be used for determining soil thermal resistivity have been developed. For this purpose, experimental results for clay, silt, silty-sand, fine- and coarse-sands have been used. Individual ANN models, applicable to each of these soils and consisting of two input parameters (moisture content and dry density) were developed. While, the generalized ANN model, applicable to any soil, consists of six input parameters (D_{10}, D_{30}, D_{50}, D_{70}, moisture content, dry density). All these models have one output parameter, the soil thermal resistivity. It has been demonstrated that these ANN

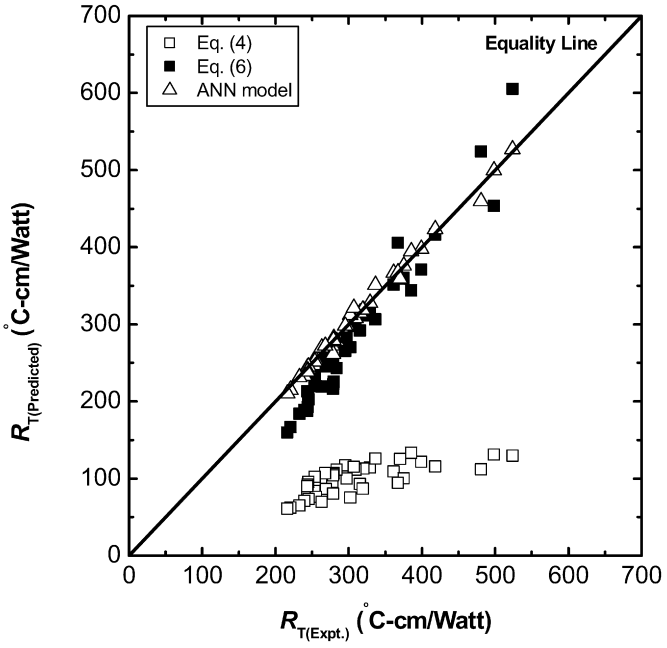

Fig. 19. Comparison of the results obtained from the individual ANN models and empirical relationships.

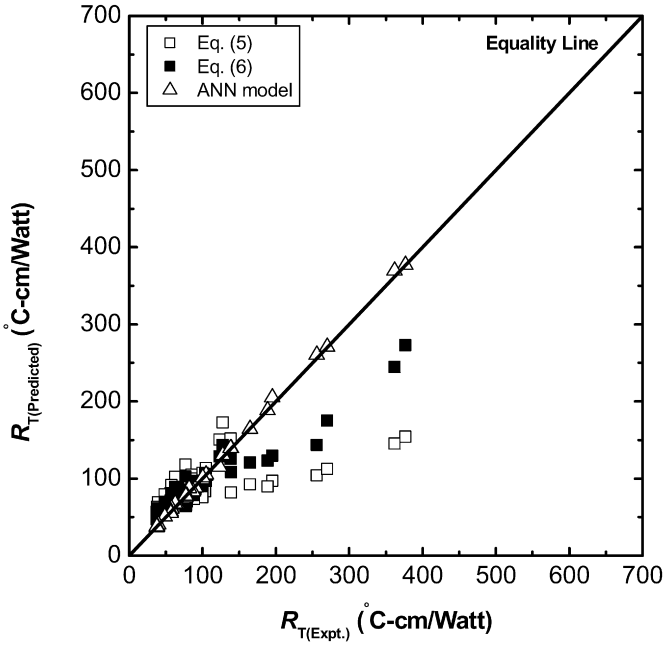

Fig. 21. Comparison of the results obtained from the individual ANN models with empirical relationships.

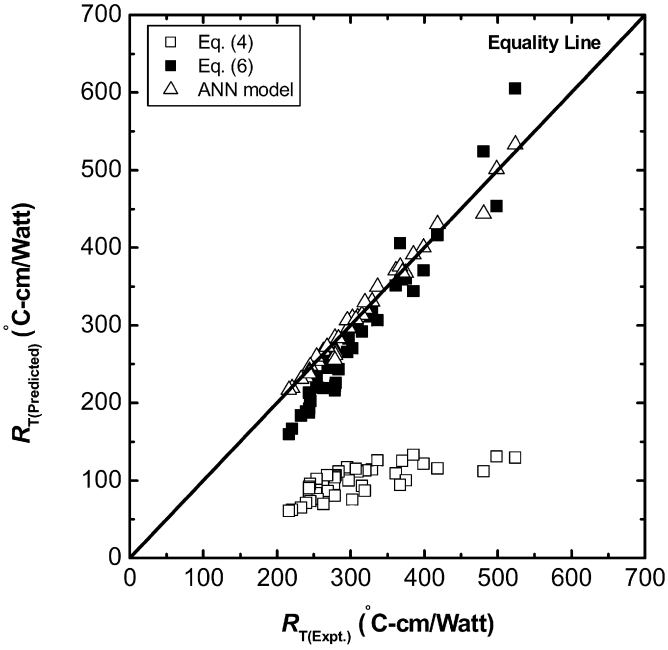

Fig. 20. Comparison of the results obtained from the model ANN-G and empirical relationships.

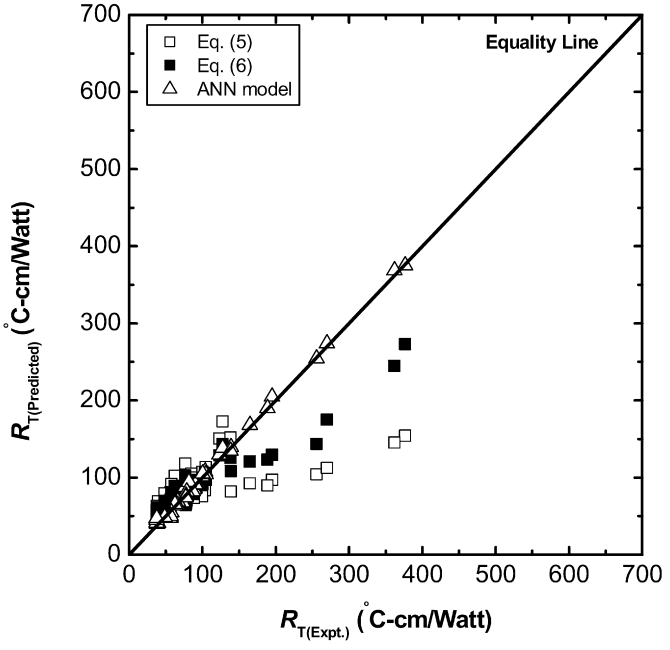

Fig. 22. Comparison of the results obtained from the model ANN-G with empirical relationships.

models are quite efficient in determining thermal resistivity of various soils and yield thermal resistivity values that match very well with those obtained experimentally. The ANN models are found to yield better soil thermal resistivity as compared to the results obtained by employing the relationships available in the literature. However, the study highlights the superiority of the generalized ANN model over individual ANN models, for determining thermal resistivity of any type of soil compacted to a given state.

References

[1] M.S. Kerstan, Thermal properties of soils, Engineering Experiment Station Bulletin 28, University of Minnesota, Minneapolis, 1949.

[2] M. Van Rooyen, Soil thermal resistivity, Doctoral Thesis, Princeton University, New Jersey, 1958.

[3] G.F. Tagg, Earth Resistances, George Newnes Limited, UK, 1964.

[4] M.V.B.B. Gangadhara Rao, Soil thermal resistivity, M. Tech. Thesis, Department of Civil Engineering, IIT Bombay, 1998.

[5] M. Van Rooyen, H.F. Winterkorn, Theoretical and practical aspects of the thermal conductivity of soils, and similar granular systems, Bulletin no. 159, U.S. Highway Research Board, 1957, pp. 58–135.
[6] D.N. Singh, K. Devid, Generalized relationships for estimating soil thermal resistivity, Experimental Thermal and Fluid Science 22 (2000) 133–143.
[7] A. Dalinaidu, D.N. Singh, A field probe for measuring thermal resistivity of soils, Journal of Geotechnical and Geoenvironmental Engineering 130 (2) (2004) 213–216.
[8] N.K. Flood, Neural networks in civil engineering—1: Principles and understanding, Journal of Computing in Civil Engineering 8 (2) (1994) 131–148.
[9] N.K. Flood, Neural networks in civil engineering—2: Principles and understanding, Journal of Computing in Civil Engineering 8 (2) (1994) 149–162.
[10] J.M. Zurada, Introduction to artificial neural systems, West. St. Paul, MN, 1992.
[11] L.V. Fausett, Fundamentals of Neural Networks: Architecture, Algorithms, and Applications, Prentice-Hall, Englewood Cliffs, NJ, 1994.
[12] M.T. Hagan, H.B. Demuth, M. Beale, Neural Network Design, Thomson Learning, Singapore, 2002.
[13] P. Orbanić, M. Fajdiga, A neural network approach to describing the fretting fatigue in aluminum–steel couplings, International Journal of Fatigue 25 (2003) 201–207.
[14] A.T.C. Goh, Seismic liquefaction potential assessed by neural networks, Journal of Geotechnical and Geoenvironmental Engineering 120 (9) (1994) 1467–1480.
[15] H. Sonmez, C. Gokceoglu, H.A. Nefeslioglu, A. Kayabasi, Estimation of rock modulus: For intact rocks with an artificial neural network and for rock masses with a new empirical equation, International Journal of Rock Mechanics and Mining Sciences 43 (2) (2005) 224–235.
[16] R. Hecht-Nielsen, Kolmogorov's mapping neural network existence theorem, in: Proceedings of the first IEEE international conference on neural networks, San Diego, CA, USA, 1987, pp. 11–14.
[17] D.R. Hush, Classification with neural networks: a performance analysis, in: Proceedings of the IEEE International Conference on Systems Engineering, Dayton, OH, USA, 1989, pp. 277–280.
[18] M. Boyd, I. Kaastra, Designing a neural network for forecasting financial and economic time series, Neurocomputing 10 (3) (1996) 215–236.
[19] I. Kanellopoulas, G.G. Wilkinson, Strategies and best practice for neural network image classification, International Journal of Remote Sensing 18 (1997) 711–725.
[20] M.A. Grima, R. Babuska, Fuzzy model for the prediction of unconfined compressive strength of rock samples, International Journal of Rock Mechanics and Mining Science 36 (1999) 339–349.
[21] M.E. Haque, K.V. Sudhakar, ANN back-propagation prediction model for fracture toughness in microalloy steel, International Journal of Fatigue 24 (2002) 1003–1010.
[22] D.H. Rumelhart, G.E. Hinton, R.J. Williams, in: D.E. Rumelhart, J.L. McClelland (Eds.), Learning internal representation by error propagation: Parallel distributed processing, vol. 1, MIT Press, Cambridge, MA, 1986 (Chapter 8).
[23] Y.M. Najjar, I.A. Basheer, W.A. Naouss, Neural modelling of Kansas soil swelling, Transportation Research, Record No. 1526, 1996, pp. 14–19.
[24] H. Kim, A.F. Rauch, C.T. Haas, Automated quality assessment of stone aggregates based on laser imaging and a neural network, Journal of Computing in Civil Engineering 18 (1) (2004) 58–64.
[25] T.N. Singh, A.R. Gupta, R. Sain, A comparative analysis of cognitive systems for the prediction of drillability of rocks and wear factor, Geotechnical and Geological Engineering 24 (2006) 299–312.
[26] S.K. Das, P.K. Basudhar, Prediction of coefficient of lateral earth pressure using artificial neural networks, Electronic Journal of Geotechnical Engineering, 10—Bundle A (2005) paper 0506.
[27] A.T.C. Goh, Back-propagation neural networks for modelling complex systems, Artificial Intelligence in Engineering 9 (1995) 143–151.
[28] A.T.C. Goh, Modelling soil correlations using neural networks, Journal of Computing in Civil Engineering 9 (4) (1995) 275–278.
[29] M.A. Shahin, M.B. Jaksa, H.R. Maier, Predicting the settlement of shallow foundations on cohesionless soils using back-propagation neural networks, Research Report No. R167, The University of Adelaide, Adelaide, 2000.
[30] M.A. Shahin, M.B. Jaksa, H.R. Maier, Artificial neural network applications in geotechnical engineering, Australian Geomechanics 36 (1) (2001) 49–62.
[31] F. Amegashie, J.Q. Shang, E.K. Yanful, W. Ding, S. Al-Martini, Using complex permittivity and artificial neural networks to identify and classify copper, zinc, and lead contamination in soil, Canadian Geotechnical Journal 43 (2006) 100–109.
[32] J.J. Shi, Reduction prediction error by transforming input data for neural networks, Journal of Computing in Civil Engineering 18 (2) (2000) 105–114.
[33] M.A. Shahin, H.R. Maier, M.B. Jaksa, Data division for developing neural networks applied to geotechnical engineering, Journal of Computing in Civil Engineering 18 (2) (2004) 105–114.
[34] M. Banimahd, S.S. Yasrobi, P.K. Woodward, Artificial neural network for stress–strain behavior of sandy soils: Knowledge based verification, Computers and Geotechnics 32 (2005) 377–386.
[35] M.A. Shahin, M.B. Jaksa, Neural network prediction of pullout capacity of marquee ground anchors, Computers and Geotechnics 32 (2005) 153–163.
[36] H. Demuth, M. Beale, M. Hagan, Neural Network Toolbox User's Guide, The Math Works, Inc., Natick, MA, USA, 2006.
[37] M.V.B.B. Gangadhara Rao, D.N. Singh, A generalized relationship to estimate thermal resistivity of soils, Canadian Geotechnical Journal 36 (4) (1999) 767–773.
[38] F.C. Hooper, F.R. Lepper, Transient heat flow apparatus for the determination of thermal conductivity, Journal of American Society of Heating and Ventilating Engineers (1950) 129–140.
[39] J.K. Mitchell, T.C. Kao, Measurement of soil thermal resistivity, Journal of the Geotechnical Engineering Division, ASCE 104 (10) (1978) 1307–1320.
[40] A. Dalinaidu, D.N. Singh, A generalized procedure for determining thermal resistivity of soils, International Journal of Thermal Sciences 43 (1) (2004) 43–51.
[41] J.M. Twomey, A.E. Smith, Validation and verification, in: N. Kartam, I. Flood, J.H. Garret (Eds.), Artificial Neural Networks for Civil Engineers: Fundamentals and Applications, ASCE, New York, 1997, pp. 44–64.
[42] M. Stone, Cross-validatory choice and assessment of statistical predictions, Journal of Royal State Society B 36 (1974) 111–147.
[43] K. Hornik, M. Stinchcombe, H. White, Multilayer feed forward networks are universal approximators, Neural Networks 2 (1989) 359–366.
[44] M.G. Sakellariou, M.D. Ferentinou, A study of slope stability prediction using neural networks, Geotechnical and Geological Engineering 23 (2005) 419–445.
[45] C. Gokceoglu, K. Zorlu, A fuzzy model to predict the uniaxial compressive strength and the modulus of elasticity of a problematic rock, Engineering Applications of Artificial Intelligence 17 (2004) 61–72.
[46] M.A. Grima, R. Babuska, Fuzzy model for the prediction of unconfined compressive strength of rock samples, International Journal of Rock Mechanics and Mining Science 36 (1999) 339–349.
[47] J. Finol, Y.K. Guo, X.D. Jing, A rule based fuzzy model for the prediction of petrophysical rock parameters, Journal of Petroleum Science and Engineering 29 (2001) 97–113.
[48] C. Gokceoglu, A fuzzy triangular chart to predict the uniaxial compressive strength of Ankara agglomerates from their petrographic composition, Engineering Geology 66 (2002) 39–51.
[49] Y. Erzin, Artificial neural networks approach for swell pressure versus soil suction behavior, Canadian Geotechnical Journal 44 (2007) 1–9, doi:10.1139/T07-052.
[50] Y. Yukselen, Y. Erzin, Artificial neural networks approach for zeta potential of montmorillonite in the presence of different cations, Environmental Geology (2007), published online 16 July 2007, doi:10.1007/s00254-007-0872-x.